

**Modeling of a thermally integrated 10 kW<sub>e</sub> planar solid oxide fuel cell  
system with anode offgas recycling and internal reforming  
by discretization in flow direction**

**Stefanie Wahl<sup>a,\*</sup>, Ana Gallet Segarra<sup>a</sup>, Peter Horstmann<sup>a</sup>, Maxime Carré<sup>a</sup>,**

**Wolfgang G. Bessler<sup>b,c</sup>, François Lapique<sup>d</sup>, K. Andreas Friedrich<sup>c</sup>**

*\*corresponding author: Stefanie.Wahl2@de.bosch.com, tel.: +49 711 811 42832, fax: +49 711 811 518 42832*

<sup>a</sup> **Robert Bosch GmbH, D-71701 Schwieberdingen, Germany**

<sup>b</sup> **Institute of Energy System Technology (INES), Offenburg University of Applied Sciences, D-77652 Offenburg, Germany**

<sup>c</sup> **German Aerospace Center (DLR), D-70569 Stuttgart, Germany**

<sup>d</sup> **LRGP, CNRS – Université de Lorraine, F-54001 Nancy, France**

**Abstract**

Combined heat and power production (CHP) based on solid oxide fuel cells (SOFC) is a very promising technology to achieve high electrical efficiency to cover power demand by decentralized production. This paper presents a dynamic quasi 2D model of an SOFC system which consists of stack and balance of plant and includes thermal coupling between the single components. The model is implemented in Modelica<sup>®</sup> and validated with experimental data for the stack *UI*-characteristic and the thermal behavior. The good agreement between experimental and simulation results demonstrates the validity of the model. Different operating conditions and system configurations are tested, increasing the net electrical efficiency to 57 % by implementing an anode offgas recycle rate of 65 %. A sensitiv-

ity analysis of characteristic values of the system like fuel utilization, oxygen-to-carbon ratio and electrical efficiency for different natural gas compositions is carried out. The result shows that a control strategy adapted to variable natural gas composition and its energy content should be developed in order to optimize the operation of the system.

*Keywords: Solid oxide fuel cell (SOFC), system, modeling, dynamic, two-dimensional (2D)*

## **1 Introduction**

The share of power produced by combined heat and power generation (CHP) in Germany has to be increased by more than 25 % by the year 2020 [1] in order to fulfill the plans regarding energy efficiency and the reduction of primary energy consumption. Concerning the total efficiency, that means the sum of electrical and thermal efficiency, decentralized power production is more efficient than that in centralized power plants since the heat can be used close to the production site, for example, in residential buildings or as process heat for industrial applications. CHP based on solid oxide fuel cells (SOFC) is a very promising technology to achieve high electrical efficiency since it is in the same range as that of large combined-cycle power plants.

A detailed knowledge of the behavior of all components in a complex SOFC system regarding temperature and concentration distribution is required to achieve optimal electrical efficiency and minimal heat loss at different operating conditions. Several investigations have already dealt with the modeling of SOFC systems without implementing spatial discretization, so called 0D or lumped models [2]-[8]. An improvement of these system models can be achieved by using a discretization of the stack, for example in flow direction [9, 10]. Furthermore the stack can be also discretized by using a 1D+1D model [11, 12], a 2D [13] or a 3D model [14]. In a 1D + 1D model, the component is discretized in flow direction and also divided in different layers perpendicular to the flow, corresponding to each volume chamber and/or solid layer. In addition to that, many researchers have shown the impact of a discretization of the whole system due to a higher accuracy of the results because detailed information along flow direction is needed for different physical calculations [15]-[17]. In particular, co- and counter-flow heat exchangers can be distinguished from each other. Additionally, if the model is validated

once, other configurations can be tested easily and a simple change of parameters is possible because of their physical modeling.

Since a discretized system model appears necessary for a number of reasons, the goal of this study is the investigation of the whole electrochemical and thermal system with a discretization in flow direction. We focus on the dynamic modeling and simulation of a SOFC system for CHP application. The system includes an SOFC stack and balance of plant (BoP) like heat exchangers, pre-reformer, burner, pipes and blowers. Compared to the other approaches reported in the literature, the heat transfer coefficients are calculated by using Nusselt correlations in order to simulate the thermal behavior for different operating conditions, for example, partial load. Additionally, each component of the system is discretized in flow direction and the quality of the model is evaluated by validation with experimental data. With the presented quasi 2D model, different operating conditions and system configurations are tested in order to maximize the net electrical efficiency of the SOFC system. A sensitivity analysis of several characteristic values of the system is carried out to consider the influence of different natural gas compositions.

## 2 System Layout

The main components of the SOFC system studied here are shown in Figure 1. SOFC systems are usually operated with natural gas. The gas is fed to the system and has to be heated before entering the pre-reformer. In the pre-reformer the longer alkanes contained in natural gas are converted into a hydrogen-rich gas in order to avoid carbon deposition inside the stack. The reformed gas enters the anode side of the SOFC stack and reacts electrochemically with the oxygen ions transferred from the cathode to the anode through the electrolyte. After leaving the stack, part of the anode offgas can be recycled in order to increase the fuel utilization of the system and therefore the electrical efficiency. The ratio of the recirculated flow  $\dot{n}_{rec}$  to the anode offgas  $\dot{n}_{an,out}$  can be defined as the recycle ratio *rec* with the following equation:

$$rec = \frac{\dot{n}_{rec}}{\dot{n}_{an,out}} \quad (1)$$

The other fraction of the anode flue gas and the cathode offgas are fed to the burner where complete combustion takes place. The flue gas is then used to heat up the gas and air flow. Each component is thermally integrated as well as possible in order to minimize heat loss and to achieve high efficiency. For the calculation of the gross electrical efficiency  $\eta_{DC}$  only the electrical power  $P_{DC}$  produced by the SOFC stack is considered. It is related to the energy input of the system which is calculated using the flow of natural gas entering the system  $\dot{n}_{NG,in}$  and its lower heating value  $LHV_{NG,in}$ :

$$\eta_{DC} = \frac{P_{DC}}{\dot{n}_{NG,in} \cdot LHV_{NG,in}} \quad (2)$$

The net electrical efficiency  $\eta_{AC}$  takes into account the conversion losses of the inverter and the power consumption of the blowers  $P_{bl}$ :

$$\eta_{AC} = \frac{P_{DC} \cdot \eta_{inv} - P_{bl}}{\dot{n}_{NG,in} \cdot LHV_{NG,in}} \quad (3)$$

For the calculation an inverter efficiency  $\eta_{inv}$  of 0.95 is assumed. The power consumption of the blowers is calculated by using the volume flow rate  $\dot{V}_{fl}$  and the pressure drop  $\Delta p$  in a single component (equation 9) :

$$P_{bl} = \Delta p \cdot \dot{V}_{fl} \quad (4)$$

To evaluate the lifetime of the system different characteristic values are used. The fuel utilization of the stack ( $FU_{Stack}$ ) is limited because otherwise the fuel starvation would cause degradation of the stack. To calculate the  $FU_{Stack}$  the following equation is used:

$$FU_{Stack} = \frac{I \cdot N_{cell}}{F \cdot \dot{n}_{an,in} \cdot \sum_k x_k \cdot N_{k,e^-}} \quad (5)$$

Where  $I$  is the electrical current,  $N_{cell}$  is the number of cells of the stack and  $N_{k,e^-}$  describes the number of transferred electrons in the electrochemical reaction of the specie  $k$ . Furthermore, the Faraday constant  $F$  is used.

Another important parameter for the lifetime of SOFC systems with anode offgas recycling is the oxygen-to-carbon ratio (OTCR). It is defined by the amount of oxygen and carbon atoms in the fuel:

$$\text{OTCR} = \frac{x_{\text{H}_2\text{O}} + x_{\text{CO}} + 2 \cdot x_{\text{CO}_2}}{n \cdot x_{\text{C}_n\text{H}_{2n+2}} + x_{\text{CO}} + x_{\text{CO}_2}} \quad (6)$$

A low OTCR can cause carbon deposition since there is not enough water for the steam reforming of alkanes. The higher the OTCR, the higher the dilution of the fuel and this decreases the Nernst voltage. Therefore the OTCR should be chosen carefully to achieve a compromise between safety and efficiency.

### 3 Modeling Approach

The model is built up in the simulation tool SimulationX<sup>®</sup> which is based on the modeling language Modelica<sup>®</sup>. It is an object-oriented language for multi-physical modeling of equations considering thermodynamic properties, chemical reactions and heat transfer. The main advantage of this tool is the calculation of closed cycle processes, for example, thermally and chemically integrated fuel cell systems. Additionally, complex systems with recycle loop and counter-flow components like heat exchangers or stacks can be computed. A component library has been built up, so that each component shown in Figure 1 is modeled by using the same basic blocks. The dynamic behavior of the single components includes heat transfer and chemical reactions in pre-reformer and stack. The model is a so called quasi-2D model. On the one hand it is discretized in flow direction and on the other hand it is spatially resolved due to the use of different blocks for heat transfer mechanisms. Each block represents a single slice of the geometry.

The model is based on the following assumptions. We assume that all species and the mixture of them act as ideal gases. The single components are discretized in flow direction and each compartment acts as a continuous stirred tank reactor (CSTR). Furthermore the electrodes and current collectors act as isopotential surfaces.

For full load operation the geometric and operating parameters of the single components are shown in Table 1.

#### 3.1 General structure of a single component

The schematic of an elemental component is shown in Figure 2. It consists of a volume chamber dis-

cretized in single compartments. In each of them the thermodynamic state properties are calculated by using mass, momentum, and energy balances. If the component is a simple pipe there is a heat loss  $\dot{Q}_{\text{loss}}$  to the environment. For more complex components like the pre-reformer or a heat exchanger, heat transfer  $\dot{Q}_{\text{hex}}$  between two fluids takes place – one at the inside and one at the outside of the chamber. Each component is modeled by combining single blocks (Figure 3) which is possible due to its modular structure. The fluid enters the volume chamber which is thermally connected to the mass. The heat transfer mechanisms which take place in this case are forced convection and conduction through the wall. There is a heat transfer between the thermal mass and the environment. For the calculation free convection is considered. An insulation layer can be added in order to reduce the heat flux to the ambient air.

The mass balance in each compartment  $i$  is given by

$$\frac{dn_i}{dt} = \dot{n}_{i-1} - \dot{n}_i + \sum_k \nu_{kj} \cdot r_{j,i} \quad (7)$$

In the above mentioned equation,  $\nu_{kj}$  is the stoichiometric coefficient of the specie  $k$  in the chemical reaction  $j$  and  $r_{j,i}$  describes the rate of the reaction  $j$  in the compartment  $i$ . If the kinetic and potential energies are neglected, the energy balance results as follows:

$$n_i c_{p,m,i} \frac{dT_i}{dt} = \dot{n}_{i-1} \cdot h_{m,i-1} - \dot{n}_i \cdot h_{m,i} + \sum \dot{Q}_i + \sum W_i \quad (8)$$

In this equation the enthalpy of each species  $h_m$  is calculated by using the NASA polynomials [18].

The model presented here also includes pressure losses in each compartment. These are calculated according to the Bernoulli equation which is combined with the Darcy-Weisbach equation for flow involving friction [19]:

$$\Delta p = \frac{1}{2} \rho v^2 \left( \lambda \frac{L/N}{d_h} + \zeta \right) \quad (9)$$

Where  $\rho$  is the density and  $v$  the velocity of the fluid. Furthermore,  $\lambda$  is the friction factor and  $\zeta$  is the friction factor for additional losses due to manifolds.

The thermodynamic properties like density, heat capacity, and thermal conductivity of the fluid are

calculated by using higher-order polynomials [20]. The hydraulic diameter  $d_h$  involved in equation (9) is calculated by using the cross section area  $A$  and the wetted perimeter  $u$ :

$$d_h = \frac{4A}{u} \quad (10)$$

### 3.2 Heat exchanger

The heat exchanger is used for heating the fluids to process temperature by the use of hot flue gas. Different geometries can be considered to find the optimal design of a heat exchanger: plate, double-pipe, or tube bundle heat exchanger. The following equation expresses the transferred heat  $\dot{Q}_{\text{trans},i}$  in the considered tubular device:

$$\dot{Q}_{\text{trans},i} = k_{\text{trans},i} \cdot A_{\text{ref},i} \cdot (T_{1,i} - T_{2,i}) \quad (11)$$

The heat transmission coefficient  $k_{\text{trans}}$  can be calculated by using the heat transfer coefficient at the inner  $h_{\text{is}}$  and outer side  $h_{\text{os}}$  of the wall and the thermal conduction  $k_{\text{cond}}$  through the solid material:

$$(k_{\text{trans},i} \cdot A_{\text{ref},i})^{-1} = \frac{1}{h_{\text{is},i} \cdot A_{\text{is},i}} + \frac{\ln(d_{\text{out}}/d_{\text{in}})}{k_{\text{cond},s} \cdot 2\pi L_i} + \frac{1}{h_{\text{os},i} \cdot A_{\text{os},i}} \quad (12)$$

$$h_i = \frac{\text{Nu}_i \cdot k_{\text{cond},\text{fl},i}}{L_{\text{char}}} \quad (13)$$

At the inner wall of each component forced convection occurs. The heat transfer coefficient in each discretization compartment is calculated by using empirically-determined Nusselt correlations [21][22]. Since the considered heat exchanger consists of an irregular geometry with laminar flow, the Nusselt correlation has to be modified [23]. Therefore a general approach for the Nusselt correlation depending on the Reynolds number  $\text{Re}$  and the Prandtl number  $\text{Pr}$  in the form

$$\text{Nu}_i = C \cdot \text{Re}_i^m \cdot \text{Pr}_i^n \quad (14)$$

is used with experimentally determined constant  $C$  and exponents  $m$  and  $n$  (see Table 3).

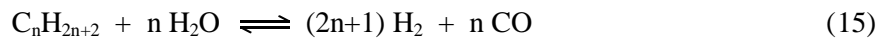
The experiments were carried out for different flow rates of fuel and air and the result of the validation is shown in section 4.4. At the outer wall of a single component either free convection or forced convection takes place. Depending on the kind of heat transfer, either a heat loss to the environment or

heat exchange with another fluid from a neighbored component occurs. These experimentally determined parameters were used for the calculation of the heat transfer in all components in the mentioned components *gas processor* in Figure 1.

### 3.3 *Pre-reformer*

SOFC systems which are fed with natural gas need reforming to obtain a hydrogen-rich gas mixture. The reforming reactions can either take place at the anode of the SOFC stack or in a pre-reformer. We extend the model of a single heat exchanger by including chemical reactions in order to calculate the dynamic behavior of the different gas concentrations in the system. There are different possibilities to reform natural gas: partial oxidation, dry, and steam reforming [24]. Since higher electrical efficiencies can be achieved by systems which operate with steam reforming, this alternative has been chosen for the system. The chemical equilibrium is influenced by the water-gas-shift reaction as well, equations see Table 4. The reaction rates are determined by using the kinetics of each equation taking into account catalyst amount, pressure, and concentrations. The used equations and constants for the reaction rates can be found in [25]. Each reaction rate is temperature dependent and calculated dynamically.

Higher alkanes like ethane, propane, and butane have to be completely reformed before entering the stack. Otherwise they will cause carbon deposition resulting in an increase in pressure loss and damage of the stack [26]. The general stoichiometry of alkane steam reforming is given by



### 3.4 *Burner*

After leaving the stack, the anode offgas contains large molar fractions of carbon monoxide and hydrogen. Part of the offgas can therefore be recycled (see Figure 1) to increase the efficiency and the rest is burned before leaving the system. Since the simulation model is transient and start-up processes are simulated, also the combustion of methane is regarded. In Table 5 the chemical reactions for the complete combustion of CO, CH<sub>4</sub>, and H<sub>2</sub> are shown. The generated heat is used for the endothermic



reforming reactions and the heating of the fluids. The burner is modeled by using two chambers: one for the combustion and a separate one for the heat exchange.

### 3.5 Stack

The SOFC stack mainly consists of an interconnect in which two channels for air and fuel are integrated and a PEN (Positive Electrolyte Negative). This layered compound structure includes cathode, electrolyte, and anode. Together with the basic blocks for heat exchange and reformer, it results in a single cell model. The model of the stack consists of multiple cells which show the same thermal and chemical behavior and two boundary cells to evaluate the influence of the boundary conditions (ambient temperature). The structure of the SOFC stack is shown in Figure 4.

At anode and cathode, respectively, the electrochemical reaction of hydrogen and oxygen is considered:



The overall reaction can be described by



Furthermore, steam reforming and water-gas-shift reaction (equations 33-35) are considered. The direct electrochemical oxidation of carbon monoxide is neglected because it is assumed that CO is converted to H<sub>2</sub> in the water-gas shift reaction, assuming thermodynamical equilibrium [27].

The current density of the stack in each discretization compartment is calculated implicitly as a function of the cell voltage. The cell voltage in each compartment  $U_{\text{cell},i}$  is the same with respect to the assumption of isopotential surfaces:

$$U_{\text{cell}} = U_{\text{cell},1} = U_{\text{cell},i} = U_{\text{cell},N} \quad (19)$$

The cell voltage is calculated taking into account the ohmic drop and the electrode overpotentials as follows:

$$U_{\text{cell},i} = U_{\text{Nernst},i} - \Delta U_{\text{act},i} - \Delta U_{\text{ohm},i} - \Delta U_{\text{conc},i} \quad (20)$$

In this expression the Nernst voltage  $U_{\text{Nernst},i}$  can be calculated with regard to the reversible ideal potential between hydrogen and oxygen, that is regardless the fugacity coefficients:

$$U_{\text{Nernst},i} = U_{0,i} - \frac{RT_i}{2F} \ln \left( \frac{p_{\text{H}_2\text{O},i}}{p_{\text{H}_2,i} p_{\text{O}_2,i}^{1/2}} \right) \quad (21)$$

The activation energy  $E_a$  which has to be overcome for electrochemical reaction is described using the activation loss  $\Delta U_{\text{act},i}$  in a modified Butler-Volmer equation [28, 29, 30]. It is used in the form:

$$\Delta U_{\text{act},i} = \frac{RT_i}{\alpha n_e F} \sinh^{-1} \left( \frac{j}{2j_{0,i}^{\text{an/ca}}} \right) \quad (22)$$

The exchange current density  $j_{0,i}^{\text{an/ca}}$  for the two reactions is calculated by using the frequency factor  $\gamma$  as follows [31, 32]:

$$j_{0,i}^{\text{an}} = \gamma_{\text{an}} \left( \frac{p_{\text{H}_2,i}}{p_{\text{ref}}} \right)^a \cdot \left( \frac{p_{\text{H}_2\text{O},i}}{p_{\text{ref}}} \right)^b \cdot \exp \left( \frac{-E_{a,\text{an}}}{RT_i} \right) \quad (23)$$

$$j_{0,i}^{\text{ca}} = \gamma_{\text{ca}} \left( \frac{p_{\text{O}_2,i}}{p_{\text{ref}}} \right)^c \cdot \exp \left( \frac{-E_{a,\text{ca}}}{RT_i} \right) \quad (24)$$

The flow of electrons through the electrode and the flow of ions in the electrolyte results in an ohmic resistance which lowers the cell voltage. The ohmic loss  $\Delta U_{\text{ohm},i}$  is derived from the resistances of the various cell components and was calculated as follows [28, 33, 34]:

$$\Delta U_{\text{ohm},i} = \left( \frac{\delta_{\text{an}}}{\sigma_{\text{an},i}} + \frac{\delta_{\text{el}}}{\sigma_{\text{el},i}} + \frac{\delta_{\text{ca}}}{\sigma_{\text{ca},i}} + \frac{\delta_{\text{ic}}}{\sigma_{\text{ic},i}} + \frac{\delta_{\text{cl}}}{\sigma_{\text{cl},i}} \right) \cdot j \quad (25)$$

where  $\delta$  is the thickness of a single layer. The conductivity  $\sigma$  of each term is calculated taking into account the porosity  $\varepsilon$  of the electrolyte and electrodes [25]:

$$\sigma_{\text{real},i} = \sigma_{\text{theo},i} \cdot (1 - \varepsilon)^{1.5} \quad (26)$$

within the expression for the theoretical conductivity [28, 30, 33, 34]:

$$\sigma_{\text{theo},i} = \frac{A}{T_i} \exp \left( \frac{B}{T_i} \right) \quad (27)$$

For the interconnect the electrical resistivity is calculated with the data reported in [35]. These values are interpolated in a temperature range between 25 and 1000 °C.

The different gas concentrations between the electrodes and the fluid generate a concentration polarization. Since the anode is thicker than the cathode, the limiting current density of the cathode is higher than the one of the anode and as a consequence the concentration loss at the cathode can be neglected [36, 37]. Thus only the concentration voltage loss  $\Delta U_{\text{conc},i}$  at the anode is considered and the following equation is used [36, 38]:

$$\Delta U_{\text{conc},i} = -\frac{RT_i}{2F} \ln\left(1 - \frac{j}{j_{\text{as},i}^{\text{an}}}\right) + \frac{RT_i}{2F} \ln\left(1 + \frac{p_{\text{H}_2,i}^{\text{an}}}{p_{\text{H}_2\text{O},i}^{\text{an}}} \frac{j}{j_{\text{as},i}^{\text{an}}}\right) \quad (28)$$

The limiting current density of the anode  $j_{\text{as},i}^{\text{an}}$  is calculated considering that the diffusion path of the molecules is equivalent to the anode thickness [36]:

$$j_{\text{as},i}^{\text{an}} = \frac{2F p_{\text{H}_2,i}^{\text{an}} D_{\text{eff}}^{\text{an}}}{RT_i \delta_{\text{an}}} \quad (29)$$

The diffusion coefficient  $D_{\text{bin}}^{\text{an}}$  is calculated by using the empirical equation [37]:

$$D_{\text{bin}}^{\text{an}} = -(4.107 \cdot x_{\text{H}_2} + 8.704) \cdot 10^{-5} \quad (30)$$

This diffusion coefficient is then adapted to other operating conditions for pressure and temperature referred to the Chapman-Enskog diffusion theory:

$$D_{\text{an}} = D_{\text{bin}}^{\text{an}} \cdot \left(\frac{T}{T_{\text{ref}}}\right)^{1.75} \cdot \left(\frac{p_{\text{ref}}}{p}\right) \quad (31)$$

For the reference conditions  $T_{\text{ref}} = 750$  °C and  $p_{\text{ref}} = 1$  atm are used. The diffusion coefficient is then adapted to the geometrical characteristics of the anode like porosity  $\varepsilon_{\text{an}}$  and tortuosity  $\tau_{\text{an}}$  by using the following equation:

$$D_{\text{eff}}^{\text{an}} = \frac{D_{\text{an}} \cdot \varepsilon_{\text{an}}}{\tau_{\text{an}}^2} \quad (32)$$

The values for the single parameters in each equation were taken from literature and are listed in Table 2.

### 3.6 *Experimental model validation*

Figure 1 shows the setup of the system which was experimentally built up as a prototype. The splitting of the flow in the system is achieved by the recycle blower shown in Figure 1 upstream of the heat exchanger. Downstream of the blower is a flow meter which allows the measurement of the recirculation flow. The recycle blower is operated in a way to ensure the desired flow rate. For example, if the recycle blower is turned off, the whole fluid flow will enter the burner directly and nothing will be recirculated. Furthermore, the burner is a regular burner (no catalytic burner). Since the nature of material has no real impact on the combustion, stainless steel has been used for construction of the burner, regardless of any catalytic activity. The thermal validation of the system (section 4.4) according to the system design presented in Figure 1 and Figure 10 has been carried out for different operation conditions. Therefore, several experiments for testing the gas processor were carried out for 14 operating points in a range for the gas flows with  $3.6 - 8.1 \text{ l min}^{-1}$  and air ratios of 7 to 8.1. For measuring temperature, thermocouples type K are used and the overpressure is measured towards environment.

The SOFC stack was tested separately in order to provide the data for the validation of the *UI*-characteristics of the fuel cell (section 4.2). Therefore, experimental results for different operating points were measured with a 50 cells short stack in counter-flow configuration in an oven. The tests were carried out for different temperatures ( $680 - 770 \text{ }^\circ\text{C}$ ) and FU (hydrogen: 30 – 50 %, reformate: 65 – 70 %).

## 4 Results and Discussion

By using the above-presented quasi-2D model, different geometries can be considered. In particular, co- and counter-flow heat exchangers or stacks can be distinguished from each other.

### 4.1 *Number of nodes and accuracy as a compromise between calculation time and accuracy*

The number of discretization compartments has a large influence on the simulation results. It can be chosen as a compromise between numerical accuracy and calculation time. The higher the number of nodes, the more precise the simulated model result. On the other hand, since the calculation time increases exponentially, it is not always recommended for a system-level simulation to discretize in a too detailed way. Figure 5 shows the simulated values for the cell voltage and the inlet temperature of the gas depending on the number of discretization compartments. This result is obtained by simulating the whole system. Therefore each component is discretized with the given number of nodes. As a consequence the influence of the discretization of each component is represented indirectly by the anode

inlet temperature of the stack and therefore by the cell voltage. Since numerous dynamic chemical and/or thermal calculations have to be carried out involving a high number of variables in each discretization compartment, the calculation time increases rapidly with a finer discretization. The optimum in this case is  $N=8$  with a deviation for the cell voltage and the anode inlet temperature both of 0.5 % compared to the result of  $N=10$ . By using only  $N=2$  discretization compartments, the deviation of the cell voltage is 8.2 % and the deviation of the anode inlet temperature is 9.2 %. However, the required calculation time for  $N=10$  is 2 times higher than for  $N=8$  and nearly 23 times higher than for  $N=2$ .

The current density depends on temperature, pressure, and concentration in a single discretization compartment. The result along the stack is presented in Figure 6. The squared symbols in Figure 6 correspond to the values for the current density  $j$  calculated by using two nodes. For an increasing number of discretization compartments the result is shown by the dotted lines. It can be observed that the profile of the current density along the stack can be described with sufficient accuracy only by using enough compartments.

#### **4.2 Validation of *UI*-characteristics in 1D**

The *UI*-characteristics of the fuel cell is validated with experimental data for different temperatures and FU. Figure 7 shows the results for a stack temperature of 720 °C operated with pure hydrogen for two different FU. The deviation between experimental and simulated results for the different FU and current densities is max. 0.6 %. For the validation with reformat gas, the maximum deviation between theory and practice is 0.9 % for the different current densities (see Figure 8). If the data for different FU are compared, it is observed that the results are more precise for higher FU values.

#### **4.3 Spatial temperature distribution along flow direction**

Since SOFC stacks are operated at high temperature and chemical reactions occur, temperature gradients along the cell appear. Figure 9 shows an example of a simulated temperature profile along the cell. For the stack temperature two effects have to be considered. On the one hand the temperature decreases due to the endothermic reforming reaction of methane. On the other hand there is a tempera-

ture increase caused by the heat generated in the electrochemical reaction at the same time. At the beginning of the stack, the cooling effect dominates, so that the temperature decreases. As soon as most of the methane is reformed, the temperature increases. These temperature gradients along the cell lead to mechanical stresses. The higher the methane content, the higher the temperature decrease. Therefore, the anode feed should not contain too much methane.

#### ***4.4 Parameterization and validation of the system under full load operation***

For the gas processor, which includes heat exchanger and burner, several experiments were carried out in order to determine the thermal behavior and the pressure losses for different operation points. This information is necessary for the modeling of the system. The schematic setup is shown in Figure 10. The ambient air is fed to the system and compressed in a blower. The blower is controlled to ensure the desired flow rate. After the compression, the air has the temperature  $T_{1, \text{air}}$  and is heated in a heat exchanger to  $T_{2, \text{air}}$ . Since only the gas processor is tested, the heated air does not enter the cathode of the stack but the burner  $T_{3, \text{air}}$ . To avoid overheating of the burner, the pipe between heat exchanger and burner is insulated insufficiently. The combustion temperature is represented by  $T_{1, \text{flue}}$ . The flue gas is used to heat the cathode air and leaves the system at temperature  $T_{2, \text{flue}}$ . The results for the temperature are shown in Figure 11. The presented temperatures correspond to those indicated in Figure 10. Since the thermocouple of the temperature measurement point  $T_{3, \text{air}}$  is not integrated directly in the combustion zone, the deviation between the simulated flame temperature and the measured combustion temperature is about 120 K. For the other temperatures in the heat exchanger, the simulated values show a maximum deviation of 5.7 % compared to the experimental data. The deviation between simulation and experimental results varies between 10 and 30 K. Figure 12 presents the comparison of the pressure loss for simulation and experimental results for the same flow rates. The maximum deviation for all operating points is 0.2 %. The thermal behavior of the whole system was also validated with a test bench under full-load operation with a mean current density of  $300 \text{ mA cm}^{-2}$ . The result of the validation is shown in Figure 13. The fuel is heated to the temperature  $T_{2, \text{fuel}}$ . Then there is a slight warming during the reforming process to  $T_{3, \text{fuel}}$ . The gas leaves the anode at the outlet temperature  $T_{4, \text{fuel}}$  and enters the burner after heat exchange. From the data we conclude that the chemical and thermal

behavior of the single components (heat exchanger, pre-reformer, stack, and burner) is modeled with sufficient accuracy since the deviation of temperature between experiments and simulations remains below 4 %.

#### **4.5 Increase in electrical efficiency by use of anode offgas recycling**

The system is designed to ensure a high thermal integration. Therefore single components are combined into larger components, for example, the gas processor includes two heat exchangers and the pre-reformer. For that reason, the heat loss is kept very low. In full-load operation the heat loss is about 17.5 %. By using the presented model different system configurations can be tested. Figure 14 shows the energy flows of an SOFC system with the above-mentioned components with an anode offgas recycle loop. The last heat exchanger is used for waste heat recovery, for example heating of domestic water (see Figure 1). By applying a recycle loop, the energy content of the gas entering the stack can be increased. For a recycle rate of 65 % and a fuel utilization of the stack of 55 % an electrical efficiency of 56.8 % can be reached.

The system operation can be further improved by varying the recycle rate. Figure 15 shows the influence of the electrical efficiency and the electrical power of the stack depending on the recycle rate and the  $FU_{\text{stack}}$ . It can be observed that each  $FU_{\text{stack}}$  is related to an optimum of recycle rate  $rec_{\text{max}}$ . The content of water in the anode channel rises with increasing recycle rates and therefore the Nernst voltage and the electrical power decrease. However the electrical efficiency increases despite the lower input of primary energy. If the recycle rate is too high, the power decrease becomes more significant and consequently the electrical efficiency is reduced. In addition, for increasing  $FU_{\text{stack}}$ , the optimal value for the recycle rate has a lower value.

#### **4.6 Influence of different gas compositions on stack voltage and FU**

The results presented above were all simulated by assuming pure methane at the input of the system. In this section the influence of a fluctuating gas composition on the SOFC system is evaluated. In the German natural gas grid, the higher heating value of the natural gas is allowed to change between 8 and 13 kWh/m<sup>3</sup> [39]. Generally, an online detection of the gas composition is not applied since it is a

complex and expensive measurement. Figure 16 shows the gas composition which enters the system, based on gas compositions given as typical reference gases in the technical standard regulating the natural gas properties in Germany [39]. It can be observed that for this example the higher heating value varies up to 11.7 %. The values for the inlet gas flow and recycle rate have been defined so that the set point of  $FU_{\text{Stack}}$  and OTCR, listed in Table 6, are fulfilled for the operation with methane. For the following simulations the inlet gas-phase composition was varied according to the time profile shown in Figure 16 while the inlet gas flow and recycle rate were kept constant. Figure 17 shows the gas composition and temperature at the inlet of the anode. The hydrogen molar fraction varies between 11 and 25 % and the temperature between 607 and 647 °C. The temperature is influenced by two effects: on the one hand, longer alkanes have higher reforming energies than methane which would lead to a lower temperature at the outlet of the pre-reformer (see Figure 18). On the other hand, longer alkanes have a higher heating value. Therefore more heat is released in the burner. Since the burner flue gas is used to preheat the inlet flows of the system, it results in a higher temperature in the stack. The consequences of the fluctuating gas compositions are shown in Figure 19, where the characteristic values of the stack over time are presented. Declared by the stack supplier, the  $FU_{\text{Stack}}$  should be kept 60% or less, otherwise starvation could occur. The minimal value of OTCR should be 1.5 in order to avoid long-term carbon formation. Due to a safety margin, a minimal OTCR of 2 was chosen [40]. It can be observed that for all gases the condition for OTCR is not fulfilled and the OTCR is always under the value of 2. This results in a reduction of the lifetime. The gross electrical efficiency achieves a maximal value of 55 % but for some gases it is reduced to 52 %. It can be concluded that a control strategy dependent on the inlet gas composition should be implemented in order to optimize the lifetime and the electrical efficiency of the system so that  $FU_{\text{Stack}}$  can be kept under 60 % and OTCR above 2.

## 5 Conclusion

In this paper a simulation model for SOFC combined heat and power systems based on the modeling language Modelica<sup>®</sup> has been presented in order to evaluate different operating conditions with focus



on achieving the maximum possible electrical efficiency. The simulated *UI*-characteristics of the cell has been validated with experimental data for different FU, temperatures, and fuels (hydrogen and reformat) with a maximum deviation of 0.9 % for reformat. In addition, the thermal behavior of the system has been validated under full-load operation with a difference between experimental and simulation data smaller than 4 %. This good agreement demonstrates the fitness of the model for subsequent analysis and model-based system design. Different operating conditions and system configurations have been evaluated. By using an anode offgas recycle loop, an increase in the electrical efficiency to up to 57 % has been achieved. The parameters of the system (FU, OTCR, and electrical efficiency) for different types of natural gas have been compared under operating conditions determined for a reference gas (in this case pure methane) and kept constant for the other gases. For gases with methane content < 90 % the lifetime requirements are not fulfilled and the electrical efficiency is reduced. In order to solve these problems a control strategy adapted to different gas compositions should be developed.

Future work will include detailed evaluations of the system dynamics regarding start-up and part-load operation. The system design will be optimized in order to lower heat loss. Finally a robust control of the system will be implemented for the purpose of minimizing the influence of the fluctuating gas composition.

<b>Nomenclature</b>		
$A$	area	$\text{m}^2$
$c_{pm}$	molar heat capacity	$\text{J mol}^{-1} \text{K}^{-1}$
$D$	diffusion coefficient	$\text{m}^2 \text{s}^{-1}$
$d$	diameter of geometry	$\text{m}$
$E_a$	activation energy	$\text{kJ mol}^{-1}$
$F$	Faraday constant ( $F = 96485 \text{ C mol}^{-1}$ )	$\text{C mol}^{-1}$
FU	fuel utilization	-
$h$	heat transfer coefficient	$\text{W m}^2 \text{K}^{-1}$
$h_m$	specific molar enthalpy	$\text{J mol}^{-1}$
$I$	current	$\text{A}$
$j$	current density	$\text{A m}^2$
$k$	thermal conductivity	$\text{W m}^{-1} \text{K}^{-1}$
$L$	length of geometry	$\text{m}$
LHV	lower heating value	$\text{J mol}^{-1}$
$\dot{n}$	molar flow	$\text{mol s}^{-1}$
$n_e$	number of transferred electrons	-
$N$	number of discretization compartments	-
Nu	Nusselt number	-
OTCR	Oxygen-to-carbon ration	-
$p$	pressure	$\text{Pa}$

$P$	electrical power	W
$Pr$	Prandtl number	-
$\dot{Q}$	heat flux	W
$r$	reaction rate	$\text{mol s}^{-1}$
$R$	universal gas constant ( $R = 8.314 \text{ J mol}^{-1} \text{ K}^{-1}$ )	$\text{J mol}^{-1} \text{ K}^{-1}$
$rec$	recycle ratio	-
$Re$	Reynolds number	-
$T$	temperature	K
$u$	wetted perimeter	M
$U$	voltage	V
$v$	velocity	$\text{m s}^{-1}$
$\dot{V}$	volume flow rate	$\text{m}^3 \text{ s}^{-1}$
$\dot{W}$	work (e.g. blower power)	W
$x$	molar fraction	-
$\alpha$	charge transfer coefficient	-
$\gamma$	frequency factor for calculation of exchange current density	-
$\delta$	thickness	M
$\varepsilon$	porosity of the material	-
$\eta$	efficiency	-
$\lambda$	friction factor	-
$\nu$	coefficients of chemical reaction	-

$\zeta$	friction factor for additional loss due to manifolds	-
$\rho$	density	$\text{kg m}^{-3}$
$\sigma$	conductivity	$\Omega^{-1} \text{m}^{-1}$
<b>super- and subscripts</b>		
0	exchange current density	-
AC	alternating current	-
act	active	-
an	anode	-
as	limiting current density	-
bin	binary	-
bl	blower	-
ca	cathode	-
char	characteristic	-
cl	contact layer	-
cond	conduction	-
DC	direct current	-
eff	effective	-
el	electrolyte	-
fl	fluid	-

<i>h</i>	hydraulic	-
<i>i</i>	number of compartments	-
ic	interconnect	-
in	inlet	-
inv	inverter	-
is	inside	-
<i>j</i>	number of reaction	-
<i>k</i>	kind of species	-
NG	natural gas	-
os	outside	-
out	outlet	-
rec	recirculated	-
ref	reference	-
s	solid	-
std	standard	-
tot	total	-
trans	transfer	-

## References

- [1] Gesetz für die Erhaltung, die Modernisierung und den Ausbau der Kraft-Wärme-Kopplung (KWKG), i. d. F. vom 12.07.2012 (BGBl. I S.1494), vom 19.03.2002 (BGBl. I S.1092).
- [2] K. H. Lee and R. K. Strand, "A system level simulation model of SOFC systems for building applications," in SimBuild 2008 - Third National Conference of IBPSA-USA, 2008.
- [3] M. Carré, "Modeling and Control of a Domestic Solid Oxide Fuel Cell (SOFC) System with Anode Recycle," doctoral thesis, Univ. Stuttgart, 2011.
- [4] K. H. Lee and R. K. Strand, "SOFC cogeneration system for building applications, part 1: development of SOFC system-level model and the parametric study," *Renew. Energy*, vol. 34, pp. 2831-2838, 2009.
- [5] K. J. Kattke and R. J. Braun, "Implementing thermal management modeling into SOFC system level design," *J. of Fuel Cell Sci. and Technol.*, vol. 8, pp. 021009.1-021009.12, 2011.
- [6] R. Kandepu, L. Imsland, B. A. Foss, C. Stiller, B. Thorud and O. Bolland, "Modeling and control of a SOFC-GT-based autonomous power system," *Energy*, vol. 32, pp. 406-417, 2007.
- [7] M. Roknii, "Thermodynamic analysis of an integrated solid oxide fuel cell cycle with a rankine cycle," *Energy Convers. and Manag.*, vol. 51, pp. 2724-2732, 2010.
- [8] M. J. Carl, "SOFC Modeling for the Simulation of Residential Cogeneration Systems," doctoral thesis, Univ. of Guelph, 2005.
- [9] D. Andersson, E. Aberg and J. Eborn, "Dynamic modeling of a solid oxide fuel cell system in Modelica," in Proc. 8th Modelica Conference, 2011.
- [10] F. Leucht, W. G. Bessler, J. Kallo, K. A. Friedrich and H. Müller-Steinhagen, "Fuel Cell System Modeling for SOFC/GT Hybrid Power Plants, Part I: Modelling and simulation framework," vol.

196, pp. 1205-1215, 2011.

[11] C. O. Colpan, "Thermal modeling of solid oxide fuel cell based biomass gasification systems," doctoral thesis, Carleton Univ., 2009.

[12] M. Henke, C. Willich, C. Westner, F. Leucht, J. Kallo, W. G. Bessler und K. A. Friedrich, „A validated multi-scale model of a SOFC stack at elevated pressure,“ Fuel Cells 13, pp. 773-780, 2013.

[13] S. Campanari and P. Iora, "Comparison of Finite Volume SOFC Models for the Simulation of a Planar Cell Geometry," Fuel Cells: From fundam. to systems, vol. 5, pp. 34-51, 2004.

[14] L. Petruzzi, S. Cocchi and F. Fineschi, "A global thermo-electrochemical model for SOFC systems design and engineering," J. of Power Sources, vol. 118, pp. 96-107, 2003.

[15] A. J. Slippey, "Dynamic Modeling and Analysis of Multiple SOFC System Configurations," doctoral thesis, Kate Gleason College of Engineering, Rochester Institute of Technology, 2009.

[16] T. Ota, M. Koyama, C. Wen, K. Yamada and H. Takahashi, "Object-based modeling of SOFC system: dynamic behavior of micro-tube SOFC," J. of Power Sources, vol. 118, pp. 430-439, 2003.

[17] C. Stiller, "Design, Operation and Control Modelling of SOFC/GT Hybrid Systems," doctoral thesis, Norwegian Univ. of Sci. and Techn., 2006.

[18] B. J. McBride, S. Gordon and M. A. Reno, "NASA Technical Memorandum 4513 - Coefficients for Calculating Thermodynamic and Transport Properties of Individual Species," National Aeronautics and Space Administration, 1993.

[19] M. Massoud, Engineering Thermofluids - Thermodynamics, Fluid Mechanics, and Heat Transfer, Berlin Heidelberg: Springer-Verlag , 2005.

[20] B. Todd and J. B. Young, "Thermodynamic and transport properties of gases for use in solid oxide fuel cell modelling," J. of Power Sources, vol. 110, pp. 186-200, 2002.

- [21] VDI-Gesellschaft Verfahrenstechnik und Chemieingenieurwesen, VDI Waermeatlas, 10th ed., Springer-Verlag Berlin Heidelberg, 2006.
- [22] F. P. Incropera and D. P. DeWitt, Fundamentals of Heat and Mass Transfer, 4th ed., John Wiley and Sons, 1998.
- [23] W. Wagner, Waermeuebertragung, 5th ed., Vogel Buchverlag, 1998.
- [24] D. Shekhawat, J. J. Spivey and D. A. Berry, Fuel Cells: Technologies for fuel processing, Elsevier, 2011.
- [25] J. Xu and G. F. Froment, "Methane steam reforming, methanation and water-gas-shift: I. intrinsic kinetics," AIChE J., vol. 35, pp. 88-96, 1989.
- [26] P. Alphonse and F. Ansart, "Catalytic coatings on steel for low-temperature propane prereforming to solid oxide fuel cell (SOFC) application," J. of Colloid and Interface Science, vol. 336, pp. 658-666, 2009.
- [27] P. Aguiar, C. S. Adjiman and N. P. Brandon, "Anode-supported intermediate temperature direct internal reforming solid oxide fuel cell. I: model-based steady-state performance," J. of Power Sources, vol. 138, pp. 120-136, 2004.
- [28] P. Lisbona, A. Corradetti, R. Bove and P. Lunghi, "Analysis of a solid oxide fuel cell system for combined heat and power applications under non-nominal conditions," Electrochimica Acta, vol. 53, pp. 1920-1930, 2007.
- [29] S. H. Chan, K. A. Khor and Z. T. Xia, "A complete polarization model of a solid oxide fuel cell and its sensitivity to the change of cell component thickness," J. of Power Sources, vol. 93, pp. 130-140, 2001.
- [30] D. Sánchez, R. Chacartegui, A. Munoz and T. Sánchez, "Thermal and electrochemical model of internal reforming solid oxide fuel cells with tubular geometry," J. of Power Sources, vol. 160, pp.



1074-1087, 2006.

[31] S. Campanari and P. Iora, "Definition and sensitivity analysis of a finite volume SOFC model for a tubular cell geometry," *J. of Power Sources*, vol. 132, pp. 113-126, 2004.

[32] P. Costamagna, A. Selimovic, M. Del Borghi and G. Agnew, "Electrochemical model of the integrated planar solid oxide fuel cell (IP-SOFC)," *Chem. Eng. J.*, vol. 102, pp. 61-69, 2004.

[33] S. A. Hajimolana, M. A. Hussain, W. Ashri Wan Daud, M. Soroush and A. Shamiri, "Mathematical modeling of solid oxide fuel cells: A review," *Renew. and Sustain. Energy Rev.*, vol. 15, pp. 1893-1917, 2011.

[34] T. Aloui and K. Halouani, "Analytical modeling of polarizations in a solid oxide fuel cell using biomass syngas product as fuel," *Appl. Therm. Eng.*, vol. 27, pp. 731-737, 2007.

[35] Thyssen Krupp VDM, "Crofer 22 H - Preliminary Material Data Sheet No. 4050," June 2008.

[36] R. J. Braun, "Optimal Design and Operation of Solid Oxide Fuel Cell Systems for Small-scale Stationary Applications," doctoral thesis, Univ. of Wisconsin-Madison, 2002.

[37] T. F. Petersen, "A Zero-Dimensional Model of a 2nd Generation Planar SOFC Using Calibrated Parameters," *Int. J. of Thermodyn.*, vol. 9, pp. 147-159, 2006.

[38] M. Sorrentino, C. Pianese and Y. G. Guezennec, "A hierarchical modeling approach to the simulation and control of planar solid oxide fuel cells," *J. of Power Sources*, vol. 180, pp. 380-392, 2008.

[39] DVGW Regelwerk, Technische Regeln, Arbeitsblatt G260: Gas quality, 2000.

[40] M. Finkenrath, „Simulation und Analyse des dynamischen Verhaltens von Kraftwerken mit oxidkeramischer Brennstoffzelle (SOFC),“ doctoral thesis, Forschungszentrum Jülich, 2005.

[41] A. Bieberle, L. P. Meier and L. J. Gauckler, "The Electrochemistry of Ni Pattern Anodes Used as Solid Oxide Fuel Cell Model Electrodes," *J. of the Electrochem. Soc.*, vol. 148, pp. A646-A656,

2001.

## Tables

Table 1: Geometric and operating parameters of the different components for full load operation

<b>parameter</b>	<b>value</b>	<b>unit</b>
$\dot{V}_{\text{fuel}}^{\text{std}}$	15	$1 \text{ min}^{-1}$
$\dot{V}_{\text{air}}^{\text{std}}$	340	$1 \text{ min}^{-1}$
$rec$	0.64	-
$T_{\text{amb}}$	25	$^{\circ}\text{C}$
$A_{\text{act,tot}}$	2.5	$\text{m}^2$
$A_{\text{hex,gas1}}$	1	$\text{m}^2$
$A_{\text{hex,gas2}}$	0.3	$\text{m}^2$
$A_{\text{hex,air}}$	0.9	$\text{m}^2$

Table 2: Parameters for the calculation of the voltage losses

<b>parameter</b>	<b>value</b>	<b>unit</b>
$\delta_{an}$	260	$\mu\text{m}$
$\delta_{ca}$	50	$\mu\text{m}$
$\delta_{el}$	10	$\mu\text{m}$
$\delta_{ic}$	1	Mm
$\varepsilon_{an}$	0.4	-
$\varepsilon_{ca}$	0.4	-
$\tau_{an}$	2.5	-
$A_{an}$	$95 \cdot 10^6$ [1]	$\text{S K m}^{-1}$
$A_{ca}$	$42 \cdot 10^6$ [1]	$\text{S K m}^{-1}$
$A_{el}$	$3.34 \cdot 10^4$ [1]	$\text{S K m}^{-1}$
$B_{an}$	-1150 [1]	K
$B_{ca}$	-1200 [1]	K
$B_{el}$	-10300 [1]	K
$a$	0.12 [2]	-
$b$	0.7 [2]	-
$c$	0.25 [2]	-
$\gamma_{an}$	$5.5 \cdot 10^8$ [3]	$\text{A m}^{-2}$
$\gamma_{ca}$	$7 \cdot 10^8$ [4]	$\text{A m}^{-2}$
$E_{a,an}$	$10 \cdot 10^4$ [3]	$\text{J mol}^{-1}$

$$E_{a,ca} \quad 11.7 \cdot 10^4 [4] \quad \text{J mol}^{-1}$$

---

Table 3: Parameters for the used Nusselt correlation in equation (14)

<b>parameter</b>	<b>value</b>	<b>unit</b>
<i>C</i>	0.57	-
<i>m</i>	0.9	-
<i>n</i>	0.3	-

Table 4: Chemical reactions for steam reforming of CH<sub>4</sub> and water gas shift reaction

<b>chemical reaction</b>	<b>reaction enthalpy</b>
$\text{CH}_4 + \text{H}_2\text{O} \rightleftharpoons 3 \text{H}_2 + \text{CO}$	$\Delta H_{\text{R}}^0 = 205.9 \text{ kJ mol}^{-1}$ (33)
$\text{CH}_4 + 2 \text{H}_2\text{O} \rightleftharpoons 4 \text{H}_2 + \text{CO}_2$	$\Delta H_{\text{R}}^0 = 164.7 \text{ kJ mol}^{-1}$ (34)
$\text{CO} + \text{H}_2\text{O} \rightleftharpoons \text{H}_2 + \text{CO}_2$	$\Delta H_{\text{R}}^0 = -41.2 \text{ kJ mol}^{-1}$ (35)

Table 5: Chemical reactions for complete combustion

<b>chemical reaction</b>	<b>reaction enthalpy</b>
$\text{CH}_4 + \text{O}_2 \rightarrow 2 \text{H}_2\text{O} + \text{CO}_2$	$\Delta H_{\text{R}}^0 = - 802.6 \text{ kJ mol}^{-1}$ (36)
$\text{CO} + 1/2 \text{O}_2 \rightarrow \text{CO}_2$	$\Delta H_{\text{R}}^0 = - 283.0 \text{ kJ mol}^{-1}$ (37)
$\text{H}_2 + 1/2 \text{O}_2 \rightarrow \text{H}_2\text{O}$	$\Delta H_{\text{R}}^0 = - 241.8 \text{ kJ mol}^{-1}$ (38)



Table 6: Reference operating conditions of the system for methane

<b>parameter</b>	<b>value</b>
$FU_{\text{Stack}}$	60 %
OTCR	2

## Figures

Figure 1: Schematic of the main components of the studied SOFC system with an anode offgas recycle loop

Figure 2: Schematic of the discretization in flow direction of a single component

Figure 3: Modular schematic of each component with single blocks

Figure 4: Quasi 2D model of the SOFC stack with boundary cells

Figure 5: Cell voltage and inlet temperature of anode for increasing number of discretization compartments, simulation results for the whole system

Figure 6: Current density along the stack for different numbers of discretization compartments

Figure 7: Validation of simulated *UI*-characteristics for hydrogen with experimental results

Figure 8: Validation of simulated *UI*-characteristics for reformat with experimental results

Figure 9: Temperature distribution along the cell

Figure 10: Schematic setup of the gas processor test

Figure 11: Validation of thermal behavior of heat exchanger and burner for different gas and air flow rates (solid line:  $\dot{V}_{\text{fuel}}^{\text{std}} = 3.6 \text{ l min}^{-1}$ , dashed line:  $\dot{V}_{\text{fuel}}^{\text{std}} = 8.1 \text{ l min}^{-1}$ )

Figure 12: Validation of pressure loss in heat exchanger and burner for different gas and air flow rates (solid line:  $\dot{V}_{\text{fuel}}^{\text{std}} = 3.6 \text{ l min}^{-1}$ , dashed line:  $\dot{V}_{\text{fuel}}^{\text{std}} = 8.1 \text{ l min}^{-1}$ )

Figure 13: Parameterization results of thermal behavior with a test bench; the solid line shows the temperatures of the fuel path, the dashed line demonstrates the air path

Figure 14: Energy flows of the system with recycle loop, referenced to the lower heating value

Figure 15: Influence of recycle rate on electrical efficiency

Figure 16: Natural gas composition and corresponding higher heating value (HHV)

Figure 17: Molar fraction and temperature of the single species entering the anode of the stack

Figure 18: Molar fraction and pre-reformer outlet temperature for a temperature of 500 °C at the inlet of the pre-reformer. The gas entering the pre-reformer has the composition shown in Figure 16 and is mixed with water in the ratio 2.5 in order to ensure an OTCR >2. The CO fraction is less than 1 %.

Figure 19:  $FU_{\text{Stack}}$ , electrical efficiency and OTCR over time, equivalent to the gas compositions shown in Figure 16

